Chapter 4
Bulk Dissipation in Nanofluid Dynamic Wetting: Wettability-Related Parameters

Abstract In this chapter, we study how nanoparticles alter the surface tension, viscosity, and rheology of nanofluids from microscopic viewpoints using molecular dynamics simulations. The results reveal the roles of additional nanoparticles on the modification of wettability-related parameters (surface tension, viscosity, and rheology) and then provide the guidelines in building nanofluid dynamic wetting models.

4.1 Introduction

The suspensions of nanoparticles in the nanofluids significantly modify the properties of the base fluids. Therefore, nanofluids exhibit attractive properties, such as high thermal conductivity and tunable surface tension, viscosity, and rheology. Various attempts have been made to understand the mechanisms for these property modifications caused by the additional nanoparticles. However, these mechanisms are still unclear due to the lack of direct nanoscale evidences.

Most previous studies on the thermophysical properties of nanofluids have explored the effects of the nanofluid parameters, such as the nanoparticle loading, diameter, and material and the base fluid type on the thermal conductivity, surface tension, viscosity, and rheology. Among these properties, the surface tension, viscosity, and rheology are related to the dynamic wetting, a process dominated by the surface tension and viscous forces. Therefore, the surface tension, viscosity, and rheology are defined as wettability-related parameters in this book. The modification of surface tension, viscosity, and rheology by adding nanoparticles greatly affects the dynamic wetting behaviors. These effects are regarded as the bulk dissipation here. Nanofluids are reported to have higher thermal conductivity than the base fluids, which were explained by several established models, e.g., Brownian motion, the solid/liquid interface layer around the nanoparticles, or the ballistic phonon transport hypotheses [1–10]. There have been many studies on thermal conductivity, but only a few studies on nanofluid surface tension, viscosity, and

G. Lu, *Dynamic Wetting by Nanofluids*,
Springer Theses, DOI 10.1007/978-3-662-48765-5_4

Table 4.1 Studies of the surface tension of nanofluids

Authors	Nanofluids	Method	σ
Zhu et al. [12]	Al_2O_3/H_2O	Experiment	Increase
Moosavi et al. [13]	ZnO/EG/glycerol	Experiment	Increase
Tanvir and Li [14]	$Al/Al_2O_3/B/MWCNT$ H_2O	Experiment	Increase
Kumar and Milanova [15]	CNT/H_2O	Experiment	Increase
Chen et al. [16]	Laponite/Fe_2O_3/ Ag/H_2O	Experiment	Constant/decrease
Das et al. [17]	Al_2O_3/H_2O	Experiment	Constant
Vafaei et al. [18]	Bi_2Te_3/AOT	Experiment/model	Decrease/increase
Murshed et al. [19]	TiO_2/H_2O	Experiment	Decrease
Radiom et al. [20]	TiO_2/H_2O	Experiment	Decrease
Liu and Kai [21]	TiN/SiC/Al_2O_3/ CNT/ammonia–H_2O	Experiment	TiN/SiC decrease Al_2O_3/CN increase

Reprinted from Ref. [11], with kind permission from Springer Science+Business Media

rheology. Table 4.1 summarizes the studies on the nanofluid surface tensions [11]. The studies are still controversial because the surface tensions of nanofluids have been reported to be increased [12–14], unchanged [15, 16], or decreased [17, 18] compared with that of the base fluids. Even for the same nanofluids, such as Al_2O_3/H_2O nanofluids, surface tension was reported to be increased by Zhu et al. [12], but unchanged by Das et al. [17]. Some studies have tried to qualitatively explain the mechanisms of these modifications in the nanofluid surface tension [14, 19–21]. Tanvir and Li [14] suggested that the attractive forces between the particles at the liquid–vapor interface increase as the particle concentration increases which increase the surface tension. However, Murshed et al. [19], Radiom et al. [20], and Liu and Kai [21] proposed that the surface tension reduction may be attributed to the reduction of the cohesive energy at the liquid–vapor interface, because nano-sized particles are brought to the lowest interfacial energy level by the Brownian motion. They also suggested that the nanoparticles function as surfactant molecules since nanoparticles are absorbed onto the liquid–vapor interface to reduce the surface tension. However, all these analyses are only suggestions without any direct evidences, and some are even contradictory.

The nanofluids are usually regarded as colloidal suspensions. Rigorously speaking, colloidal suspensions are mixture solutions containing micro-/milli-sized particles, while nanofluids containing nanosized particles. Several classical models have been proposed to predict the effective viscosity of colloidal suspensions [22–25]. However, these models failed to predict the effective viscosity of nanofluids [26–28]. The models of nanofluid viscosity have been reviewed by Eastman et al. [29], Keblinski et al. [30], and Mahbubul et al. [31]. Most of these models were only based on hypotheses or empirical correlations between the effective viscosity and macroscopic parameters, such as the loading fractions or temperatures. Some

Table 4.2 Studies of the rheology of nanofluids

Authors	Nanofluids	Method	Rheology
Das et al. [17]	Al_2O_3/H_2O, CuO/H_2O	Experiment	Newtonian
Prasher et al. [35]	Al_2O_3/PG	Experiment	Newtonian
Chen et al. [36]	TiO_2/ethylene glycol	Experiment	Newtonian
Susan-Resiga et al. [37]	Fe_3O_4/MOL	Experiment	Newtonian
Wang et al. [38]	CuO/H_2O/ethylene glycol, Al_2O_3/H_2O/ethylene glycol/engine oil	Experiment	Non-Newtonian
He et al. [39]	TiO_2/H_2O	Experiment	Non-Newtonian
Murshed et al. [40]	Al_2O_3/H_2O	Experiment	Non-Newtonian
Chen et al. [41]	TNT/EG	Experiment	Non-Newtonian (shear thinning)
Ding et al. [42]	CNT/H_2O	Experiment	Non-Newtonian (shear thinning)
Kole and Dey [43]	Al_2O_3/car coolant, CuO/gear oil	Experiment	Non-Newtonian
Yu et al. [44]	AlN/Eg, AlN/PG	Experiment	$\varphi < 5$ %: Newtonian, $\varphi > 5$ %: non-Newtonian
Yu et al. [45]	ZnO/EG	Experiment	$\varphi < 2$ %: Newtonian, $\varphi > 3$ %: non-Newtonian
Kim et al. [46]	Al_2O_3/H_2O	Experiment	$\varphi < 2$ %: Newtonian, 3 % $< \varphi <$ 5 %: non-Newtonian
Abareshi et al. [47]	α-Fe_2O_3-glycerol	Experiment	Non-Newtonian@low temperature

Reprinted from Ref. [11], with kind permission from Springer Science+Business Media

correlations had considered the effects of particle size, which is related to the Brownian motion [32, 33]; however, undetermined constants in these models must be fit from macroscopic experimental measurements. Thus, more studies are needed to identify the enhancement mechanism with microscopic evidence.

The rheological properties of nanofluids had been reviewed by Chen et al. [34]. According to the summary in Table 4.2, there is still debate about whether nanofluids exhibit Newtonian [16, 35–37] or non-Newtonian [38–47] in experiments. Even for the same nanofluid, such as Al_2O_3/H_2O nanofluids, Newtonian rheological behavior was reported by Das et al. [17] and Prasher et al. [35], while non-Newtonian rheological behavior was observed by Wang et al. [38], Murshed et al. [40], Kole and Dey [43], and Kim et al. [46]. Most of these studies mainly reported the experimental data, with few focused on the mechanisms for the rheological transformation from Newtonian to non-Newtonian fluids by adding nanoparticles. Yu et al. [45] stated that the rheological properties of nanofluids depend strongly on many factors, such as nanoparticle material, shape, the loading fractions, and temperatures. Chen et al. [34] proposed an aggregation mechanism to

interpret the rheological behavior of nanofluids and categorized the rheological behavior of nanofluids into four groups such as dilute, semi-dilute, semi-concentrated, and concentrated. However, they did not consider the mechanism of rheological transform. In addition, no direct evidence was provided to support their hypotheses.

Most previous studies of nanofluid have focused on collecting the thermophysical property data. The macroscopic measurements were then used to establish models to explain the mechanisms; however, these explanations have not been supported by direct evidence. MD simulations can provide microscopic understanding of the thermophysical properties in much greater detail, which have been extensively used to investigate the surface tension, viscosity, and rheology of pure liquids [48–55] or binary mixture solutions [56–60]. Recently, the MD simulations have also been used to model the nanofluid thermal conductivity [61–67] with some promising results that verify the theories based on macroscopic measurements. However, few MD studies have focused on the surface tension, viscosity, and rheology of nanofluids.

The objective of this chapter is to study how nanoparticles alter the surface tension, viscosity, and rheology of nanofluids from microscopic viewpoints using MD simulations. The results reveal the roles of additional nanoparticles on the modification of wettability-related parameters and then provide the guidelines in building nanofluid dynamic wetting models.

4.2 Simulation Methods

4.2.1 Simulation Systems

Figure 4.1 shows the simulated systems had four nanofluid loadings. Bulk water films (4500 water molecules) were simulated at 300 K using the molecular dynamic simulations with four gold nanoparticle loadings (φ = 0, 3.43 %, 6.77 %, and

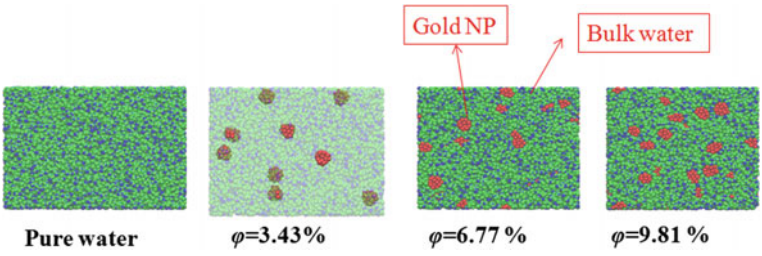

Fig. 4.1 Illustrations of the molecular structures of pure water and three gold nanoparticle nanofluid loading fractions (the water molecules are transparent to illustrate the nanoparticle positions for φ = 3.43 %). Reprinted from Ref. [11], with kind permission from Springer Science+Business Media

9.81 %). The gold nanoparticles ($0.8 \times 0.8 \times 0.8$ nm^3) randomly distributed inside the bulk liquid. The four-point TIP4P-Ew water model, PPPM technique, and SHAKE algorithm were used to describe the water–water interactions [68, 69]. The EAM [70] was used for the gold–gold interactions. The simulation details have been described in Chap. 3. A 12-6 LJ potential with σ = 3.1 Å [71] and a cutoff distance of 9 Å was used to describe the water–gold interactions. The gold nanoparticle wettability was changed with different gold–water interaction parameter ε (ε = 0.0070, 0.02714, 0.05427 and 0.08141 eV). The *NVT* ensembles at T = 300 K with a time step of 1 fs were used to calculate the thermodynamic properties. The simulations were performed with LAMMPS software packages [72].

4.2.2 Surface Tension Calculation Method

In most MD simulations, the surface tension is calculated based on Young–Laplace equation [73], as shown in Eq. (4.1).

$$\Delta p = \frac{\sigma_{\mathrm{LV}}}{R} \tag{4.1}$$

where Δp is the pressure difference between the inside and outside of the droplet, σ_{LV} is the liquid–vapor surface tension, and R is the droplet radius. However, the pressure fluctuates greatly in LAMMPS. For example, for a set pressure of 1 bar, the standard deviation of the fluctuations is about 40 bar. Thus, the surface tension cannot be calculated with such large pressure variations even with time averaging. Therefore, a new method, referred to as excess energy method here, was used to calculate the surface tension. The simulation details are shown in Chap. 3.

4.2.3 Viscosity and Rheology Calculation Method

The reverse non-equilibrium MD (rNEMD) method [74] was used to calculate the nanofluid viscosity. The method is based on Onsager linear response theory,

$$j_\alpha = -\sum_\beta L_{\alpha\beta} X_\beta \tag{4.2}$$

where j_α is the momentum flux, X_β is the driving force (velocity gradient), and $L_{\alpha\beta}$ is the diffusion coefficient (viscosity).

As shown in Fig. 4.2, a momentum flux was imposed on the bulk liquid to generate a velocity gradient. The diffusion coefficient, in this case the viscosity, was then obtained using:

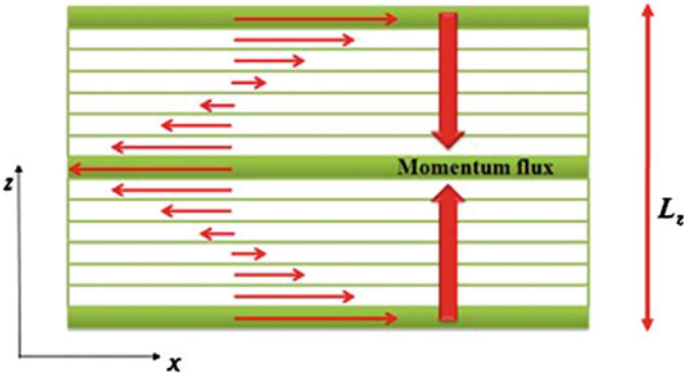

Fig. 4.2 Momentum exchange in the rNEMD simulation method. Reprinted from Ref. [11], with kind permission from Springer Science+Business Media

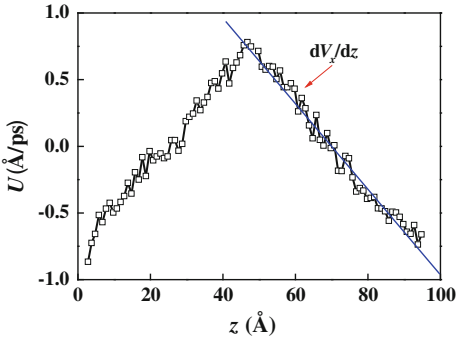

Fig. 4.3 Velocity profile in the rNEMD method. Reprinted from Ref. [11], with kind permission from Springer Science+Business Media

$$j_\alpha \langle p_x \rangle = \frac{P_x}{2tA} \tag{4.3}$$

where P_x is the pressure in the x direction, t is the velocity swapping period, and A is the area of xy plane.

To impose the momentum flux onto the bulk liquid, two water molecules were moved in the bottom and middle plates against the intended current, one with the minimum velocity and the other with the maximum velocity. The velocities were then swapped in another calculation. The momentum flux then generated a velocity gradient, dV_x/dz. As shown in Fig. 4.3, a good linear velocity profile was obtained along the z direction that was fit with a straight line with the momentum flux and then calculated using Eq. (4.3).

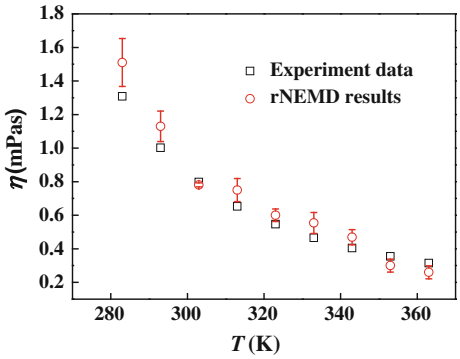

Fig. 4.4 Verification of the rNEMD method: viscosity of pure water at various temperatures. Reprinted from Ref. [11], with kind permission from Springer Science+Business Media

The velocity swapping period, t, in Eq. (4.3) was varied to create various momentum fluxes and velocities to relate the viscosity to the shear rate (rheology).

Figure 4.4 compares the present MD results with the experimental data for pure water at various temperatures. The good agreement indicates the accuracy of the present water model and the rNEMD method.

4.3 Results and Discussion

4.3.1 Surface Tension of Gold–Water Nanofluids

For pure water, the calculated surface tension from the MD simulations was $\sigma = 0.0679$ N/m at $T = 300$ K, close to the experimental value of $\sigma = 0.072$ N/m [75]. For the 3.43 % nanofluid, the addition of nanoparticles increased the surface tension for the nanoparticles with $\varepsilon_{\text{water–gold}} = 0.05427$ eV, but reduced it for those with $\varepsilon_{\text{water–gold}} = 0.0070$ eV. The different tendencies for these two cases are related to the different water–gold interactions ($\varepsilon_{\text{water–gold}}$) and water–water interactions ($\varepsilon_{\text{water–water}} = 0.0071$ eV for TIP4P-Ew). For $\varepsilon_{\text{water–gold}} < \varepsilon_{\text{water–water}}$, the nanoparticles are hydrophobic, so they tend to stay on the free surface (liquid–vapor interface), acting as surfactant-like particles, as shown in Fig. 4.5a. For $\varepsilon_{\text{water–gold}} > \varepsilon_{\text{water–water}}$, the nanoparticles are hydrophilic, so they tend to submerge into the bulk liquid, acting as non-surfactant particles, as shown in Fig. 4.5b.

The surface tension indicates the unbalanced forces acting on the liquid molecules at the interface due to the van der Waals force, as shown in Fig. 4.6a. The liquid molecules at the surface do not have an equal number of molecules in the vapor side, so they are pulled inward by the internal molecules, which results in the surface tension, pulling the liquid surface to contract to the minimum area. Thus, the nanoparticle wettability is responsible for the different surface tensions. For

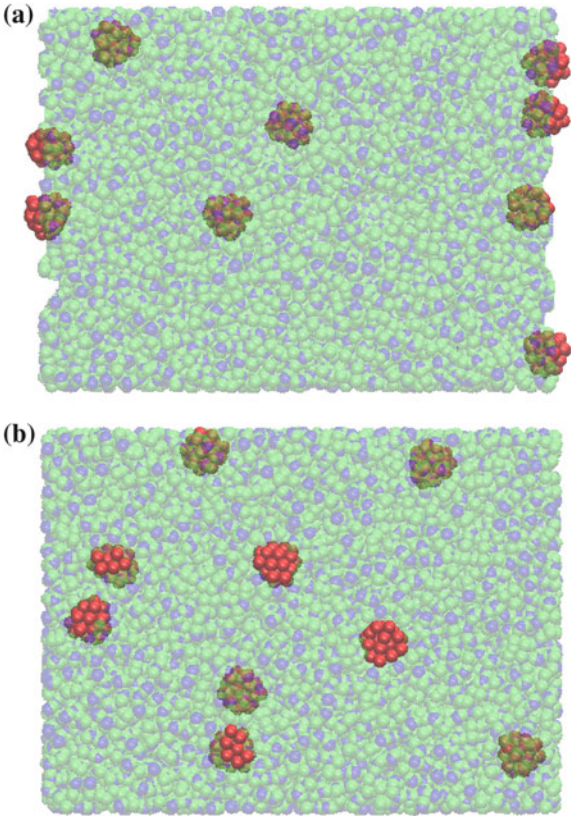

Fig. 4.5 Snapshots of the 3.43 % nanofluid with **a** hydrophobic gold nanoparticles (ε = 0.007 eV); **b** hydrophilic gold nanoparticles (ε = 0.05427 eV). Reprinted from Ref. [11], with kind permission from Springer Science+Business Media

hydrophobic nanoparticles, the nanoparticles gather on the free surface. The repulsion force between the nanoparticles and the water molecules increases the intermolecular spacing at the interface and reduces the attraction forces between the water molecules inside the bulk liquid and the ones on the free surface regions, thus reducing the surface tension, as shown in Fig. 4.6b. However, some hydrophilic nanoparticles are transported toward the interfacial region by Brownian motion where the attraction forces between the nanoparticles and the water molecules reduce the intermolecular spacing at the interface. The water molecules at the free surface are more strongly pulled inward due to the presence of the hydrophilic nanoparticles with stronger gold–water interaction forces than those with the water–water interactions, which increase the surface tension, as shown in Fig. 4.6c.

Figure 4.7 shows the evidences for the hydrophobic/hydrophilic nanoparticles changing the intermolecular spacing in the interfacial region. The water density remains constant in the bulk liquid but decreases sharply near the interface. The thickness of the reduced density region, defined as the interface width, d, decreases with increasing nanoparticle wettability, leading to the increased surface tension. In

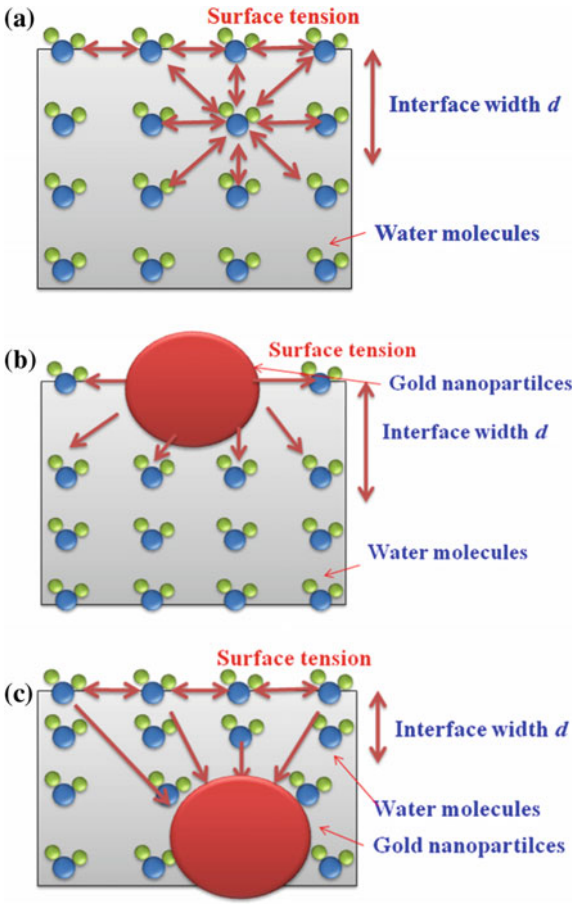

Fig. 4.6 Schematic of the van der Waals forces between water molecules and nanoparticle–water molecule near the interfacial region: **a** water molecular interaction for pure water; **b** gold nanoparticle–water molecule interactions for $\varepsilon_{water-gold} < \varepsilon_{water-water}$; **c** gold nanoparticle–water molecule interactions for $\varepsilon_{water-gold} < \varepsilon_{water-water}$. Reprinted from Ref. [11], with kind permission from Springer Science+Business Media

addition, the interface width, d, decreases with increasing φ for the hydrophilic nanoparticles, but increases with increasing φ for the hydrophobic nanoparticles.

Therefore, for nanofluids, the dynamic wetting can be facilitated by adding hydrophobic nanoparticles, but inhibited by adding hydrophilic nanoparticles, which is related to the modification of nanofluid surface tension.

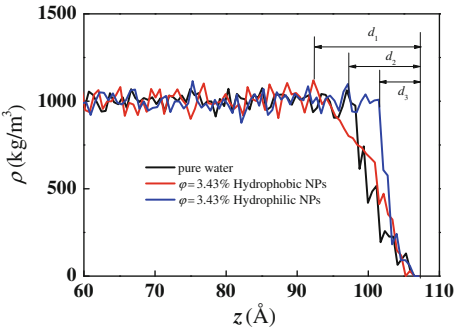

Fig. 4.7 Water density profiles perpendicular to the free surface for pure water and nanofluids with hydrophobic or hydrophilic nanoparticles (φ = 3.43 %). Reprinted from Ref. [11], with kind permission from Springer Science+Business Media

4.3.2 *Viscosity of Gold–Water Nanofluids*

Figure 4.8 shows the viscosities of pure water and low loading nanofluids (φ = 0 %, φ = 3.43 %, and φ = 6.77 %). The viscosity increases with increasing volume concentration, which agrees with experimental data [76]. The increasing viscosity with loading is illustrated by the microscopic picture of one randomly selected gold nanoparticle shown in the inset in Fig. 4.9, in which the hydrogen atoms are hidden. An absorbed water layer has formed around the gold nanoparticle, which can be observed by plotting the water density along the radial direction, as shown in Fig. 4.9. The water density near the nanoparticle at 19 Å is five times that of the bulk liquid, indicating a solid-like absorbed water layer around the gold nanoparticle. The effect can be explained by the Einstein diffusion equation [77],

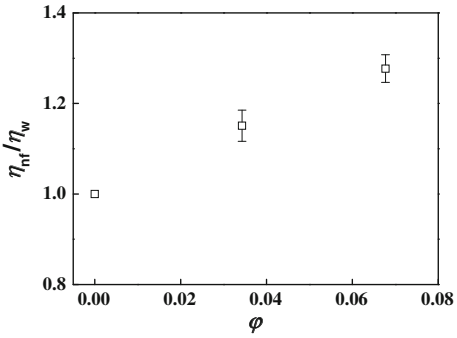

Fig. 4.8 Nanofluid viscosity for various NP loadings. Reprinted from Ref. [11], with kind permission from Springer Science+Business Media

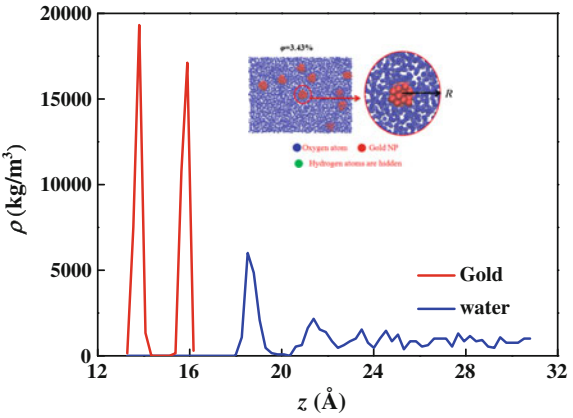

Fig. 4.9 Water density near a gold nanoparticle (*Inset* illustration of the water molecule layer). Reprinted from Ref. [11], with kind permission from Springer Science+Business Media

$$D_{\mathrm{NP}} = \frac{k_{\mathrm{B}} T}{6\pi\mu r} \tag{4.4}$$

where D_{NP} is the nanoparticle diffusion coefficient, k_{B} is Boltzmann's constant, T is the absolute temperature, μ is the base liquid viscosity, and r is the particle radius. The absorbed water layer increases the equivalent nanoparticle radius which hinders nanoparticle diffusion within the base liquid according to Eq. (4.4). Consequently, the increased nanofluid viscosity can be explained by the decreased nanoparticle diffusion coefficient. The absorbed layer is also reported as the reasons for the nanofluid thermal conductivity enhancement [51, 53]. The interactions between the nanoparticles and the water molecules were changed by modifying ε. As shown in Fig. 4.10a, the density of the absorbed water layer increases with the increasing gold–water interaction parameter. Thus, smaller diffusion coefficients occur for stronger NP–water molecule interactions, and the nanofluid viscosity can be expected to increase with increasing the gold–water interaction parameter, as shown in Fig. 4.10b. The number of gold nanoparticles in the solution affects the viscosity, as shown in Fig. 4.10b, but does not affect the intensity of the absorbed water layer for a single nanoparticle if the nanoparticle loading is low enough.

4.3.3 *Rheology of Gold–Water Nanofluids*

Figure 4.11 shows the viscosity versus shear rate variation, as known as rheological relations. For pure water and low nanofluid loadings (φ = 3.43 % and φ = 6.77 %), the viscosity remains constant for shear rates from 10^{-1} to 3×10^{2} s^{-1}. However, the viscosity of the φ = 9.81 % nanofluid remains constant only with a narrow shear rate range (from 10^{-1} to 10^{0} s^{-1}) and decreases as the shear rate increases from 10^{0} to 3×10^{2} s^{-1}, indicating shear-thinning non-Newtonian rheological behavior. This

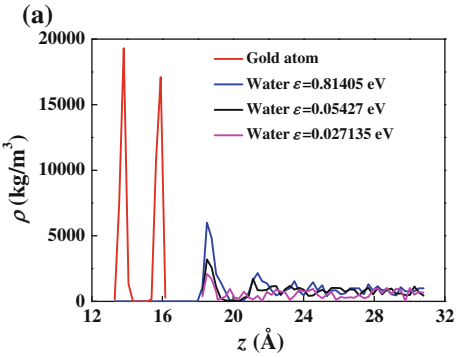

Fig. 4.10 Effects of gold nanoparticle–water molecule interactions on **a** atom number density; **b** viscosity. Reprinted from Ref. [11], with kind permission from Springer Science+Business Media

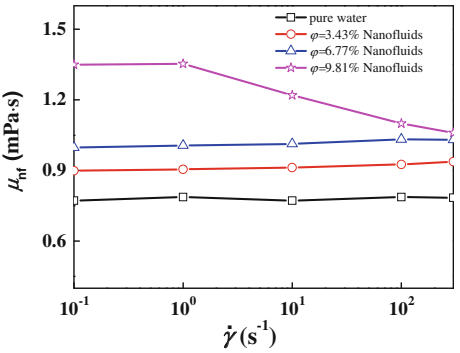

Fig. 4.11 Viscosity versus shear rate (rheology) for nanofluids for various loadings (ε = 0.05427 eV). Reprinted from Ref. [11], with kind permission from Springer Science+Business Media

rheology transformation at high shear rates was also seen experimentally by Carré and Woehl [78].

The inset in Fig. 4.12 shows a typical microscopic structure of two nanoparticle–water molecule cluster. Comparison of the particle distribution with the high loading in the inset in Fig. 4.12 with the distribution for a lower loadings seen in the

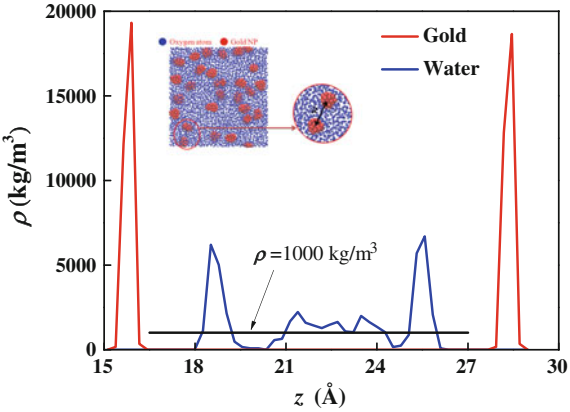

Fig. 4.12 Solidification effect at high loadings (*Inset* illustration of the molecular spacing). Reprinted from Ref. [11], with kind permission from Springer Science+Business Media

inset in Fig. 4.9 shows that there are more chances for nanoparticles to move closer together for high loadings since nanoparticles always move randomly in the base liquid due to Brownian motion. The solid-like absorbed water layers around the nanoparticles are also observed in this structure. Additionally, the water density between these two closed nanoparticles is several times larger than that of the bulk liquid density, as shown in Fig. 4.12, indicating that solidification of the water molecules also occurs in this structure, which is defined here as a solidification structure due to the additional nanoparticle–nanoparticle interactions. This solidification structure further increases the nanofluid viscosity for higher loadings. The solidification structures remain unchanged at low shear rates, where the nanofluids exhibit Newtonian rheological behavior. However, there is a critical shear rate above which the solidification structures are disrupted and the solidified water molecules move more freely, which reduces the nanofluid viscosity, leading to the shear-thinning non-Newtonian rheological behavior.

When the gold–water interactions increase for lower loadings (φ = 3.43 % and φ = 6.77 %), the viscosity increases, while the rheology remains unchanged, as shown in Fig. 4.13. Therefore, the mechanism for the solidification effect, which is more likely at high loadings, is related to but differs from the mechanism for the solid-like absorbed water layer that alters the viscosity.

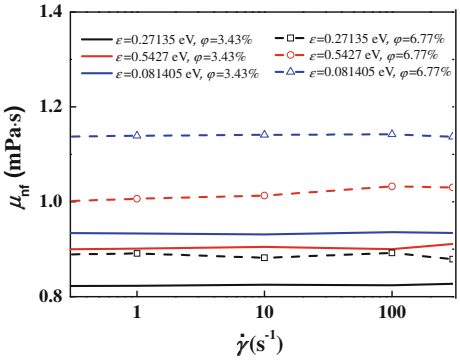

Fig. 4.13 Effects of gold nanoparticle–water molecule interactions on rheology for φ = 3.43 % and φ = 6.77 % nanoparticle loadings. Reprinted from Ref. [11], with kind permission from Springer Science+Business Media

4.4 Conclusions

The surface tension, viscosity, and rheology of gold–water nanofluids were examined using molecular dynamic simulations. The effects of the gold nanoparticle loadings and particle wettability were examined. The main conclusions are as follows:

1. The microscopic mechanism for the surface tension variation is related to the nanoparticle wettability. The repulsion of water molecules by surfactant-like nanoparticles increases the molecular spacing on the free surface which reduces the fluid surface tension. The attraction induced by non-surfactant nanoparticles reduces the molecular spacing on the free surface which increases the surface tension.
2. A solid-like absorbed water layer around the nanoparticles increases the equivalent nanoparticle radius and hinders the nanoparticle mobility within the base fluid which increases the nanofluid viscosity.
3. The nanofluid rheological behavior depends on the nanoparticle loading. For low loadings, the viscosity increases with increasing gold–water interaction forces, but remains unchanged with the shear rate, indicating Newtonian behavior. For high loadings, water molecule solidification is observed between neighboring nanoparticles due to the strong particle–particle interactions. These solidification structures are then disrupted for shear rates exceeding a critical value, which leads to shear-thinning non-Newtonian rheological behavior.

References

1. Choi SUS (1995) Enhancing thermal conductivity of fluids with nanoparticles, developments and application of non-newtonian flows. ASME, New York, FED 231/MD, vol 66, pp 99–105
2. Choi SUS (2009) Nanofluids: from vision to reality through research. J Heat Transfer 131:033106
3. Cheng LS, Cao DP (2011) Designing a thermo-switchable channel for nanofluidic controllable transportation. ACS Nano 5:1102–1108
4. Michaelides EE (2013) Transport properties of nanofluids. A critical review. J Non-Equilib Thermodyn 38:1–79
5. Chakraborty S, Padhy S (2008) Anomalous electrical conductivity of nanoscale colloidal suspensions. ACS Nano 2:2029–2036
6. Trisaksri V, Wongwises S (2007) Critical review of heat transfer characteristics of nanofluids. Renew Sustain Energy Rev 11:512–523
7. Branson BT, Beauchamp PS, Beam JC et al (2013) Nanodiamond nanofluids for enhanced thermal conductivity. ACS Nano 7:3183–3189
8. Wu S, Nikolov A, Wasan D (2013) Cleansing dynamics of oily soil using nanofluids. J Colloid Interface Sci 396:293–306
9. Murshed SMS, Leoong KC, Yang C (2008) Thermophysical and electrokinetic properties of nanofluids-A critical review. Appl Thermal Eng 28:2109–2125
10. Li YJ, Zhou JE, Tung S et al (2009) A review on development of nanofluid preparation and characterization. Powder Tech 196:89–101
11. Lu G, Duan YY, Wang XD (2014) Surface tension, viscosity, and rheology of water-based nanofluids: a microscopic interpretation on the molecular level. J Nanopart Res 16:2564
12. Zhu D, Wu S, Wang N (2010) Thermal physics and critical heat flux characteristics of Al_2O_3-H_2O nanofluids. Heat Transfer Eng 31:1213–1219
13. Moosavi M, Goharshadi EK, Youssefi A (2010) Fabrication, characterization, and measurement of some physicochemical properties of ZnO nanofluids. Int J Heat Mass Transfer 31:599–605
14. Tanvir S, Li Q (2012) Surface tension of nanofluid-type fuels containing suspended nanomaterials. Nanoscale Res Lett 7:226–236
15. Kumar R, Milanova D (2009) Effect of surface tension on nanotube nanofluids. Appl Phys Lett 94:073107
16. Chen RH, Phuoc TX, Martello D (2011) Surface tension of evaporating nanofluid droplets. Int J Heat Mass Transfer 54:2459–2466
17. Das SK, Putra N, Reotzel W (2003) Pool boiling characteristics of nano-fluids. Int J Heat Mass Transfer 46:851–862
18. Vafaei S, Purkayastha A, Jain A (2009) The effect of nanoparticles on the liquid-gas surface tension of Bi_2Te_3 nanofluids. Nanotechnology 20:185702
19. Murshed SM, Tan SH, Nguyen NT (2008) Temperature dependence of interfacial properties and viscosity of nanofluids for droplet-based microfluidics. J Phys D: Appl Phys 41:085502
20. Radiom M, Yang C, Chan WK (2010) Characterization of surface tension and contact angle of nanofluids. Proc SPIE 7522:75221D
21. Liu Y, Kai D (2012) Investigations of surface tension of binary nanofluids. Adv Mater Res 347–353:786–790
22. Einstein A (1956) Investigations on the theory of Brownian movement. Dover Publications, Inc, New York
23. Krieger IM, Dougherty TJ (1959) A mechanism for non-Newtonian flow in suspension of rigid spheres. Trans Soc Rheol 3:137–152
24. Nielsen LE (1970) Generalized equation for the elastic moduli of composite materials. J Appl Phys 41:4626
25. Batchelor GK (1977) The effect of Brownian motion on the bulk stress in a suspension of spherical particles. J Fluid Mech 83:97–117

26. Chandrasekar M, Suresh S, Chandra BA (2010) Experimental investigations and theoretical determination of thermal conductivity and viscosity of Al_2O_3/water nanofluids. Exp Thermal Fluid Sci 34:210–216
27. Nguyen CT, Desgranges F, Galanis N et al (2008) Viscosity data for Al_2O_3-water nanofluid-hysteresis: is heat transfer enhancement using nanofluids reliable. Int J Therm Sci 47:103–111
28. Lee JH, Hwang KS, Janga S et al (2008) Effective viscosities and thermal conductivities of aqueous nanofluids containing low volume concentrations of Al_2O_3 nanoparticles. Int J Heat Mass Transfer 51:2651–2656
29. Eastman JA, Phillpot SR, Choi SUS et al (2004) Thermal transport in nanofluids. Annual Rev Mater Res 34:219–246
30. Keblinski P, Eastman JA, Cahill DG (2005) Nanofluids for thermal transport. Mater Today 8:36–44
31. Mahbubul IM, Saidur R, Amalina MA (2012) Latest developments on the viscosity of nanofluids. Int J Heat Mass Transfer 55:874–885
32. Masoumi N, Sohrabi N, Behzadmehr A (2009) A new model for calculating the effective viscosity of nanofluids. J Phys D Appl Phys 42:055501
33. Hosseini SM, Moghadassi AR, Henneke DE (2010) A new dimensionless group model for determining the viscosity of nanofluids. J Therm Anal Calorim 100:873–877
34. Chen HS, Ding YL, Tan CQ (2007) Rheological behaviour of nanofluids. New J Phys 9:367
35. Prasher R, Song D, Wang J et al (2006) Measurements of nanofluid viscosity and its implications for thermal applications. Appl Phys Lett 89:133108
36. Chen HS, Ding YL, He YR et al (2007) Rheological behaviour of ethylene glycol based titanianofluids. Chem Phys Lett 444:333–337
37. Susan-Resiga D, Socoliuc V, Boros T et al (2012) The influence of particle clustering on the rheological properties of highly concentrated magnetic nanofluids. J Colloid Interface Sci 373:110–115
38. Wang XW, Xu XF, Choi SUS (1999) Thermal conductivity of nanoparticle-fluid mixture. J Thermo Heat Transfer 13:474–480
39. He Y, Jin Y, Chen HS et al (2007) Heat transfer and flow behaviour of aqueous suspensions of TiO_2 nanoparticles (nanofluids) flowing upward through a vertical pipe. Int J Heat Mass Transfer 50:2272–2281
40. Murshed SMS, Leong KC, Yang C (2008) Investigations of thermal conductivity and viscosity of nanofluids. Int J Therm Sci 47:560–568
41. Chen HS, Ding YL, Lapkin A (2009) Rheological behaviour of nanofluids containing tube rod-like nanoparticles. Powder Tech 194:132–141
42. Ding Y, Alias H, Wen D, Williams RA et al (2006) Heat transfer of aqueous suspensions of carbon nanotubes (CNT nanofluids). Int J Heat Mass Transfer 49:240–250
43. Kole M, Dey TK (2011) Effect of aggregation on the viscosity of copper oxide–gear oil nanofluids. Int J Therm Sci 50:1741–1747
44. Yu W, Xie H, Li Y et al (2011) Experimental investigation on thermal conductivity and viscosity of aluminum nitride nanofluid. Particuology 9:187–191
45. Yu W, Xie H, Chen L et al (2009) Investigation of thermal conductivity and viscosity of ethylene glycol based ZnO nanofluids. Thermochim Acta 491:92–96
46. Kim S, Kim C, Lee WH et al (2011) Rheological properties of alumina nanofluids and their implication to the heat transfer enhancement mechanism. J Appl Phys 110:34316
47. Abareshi M, Sajjadi SH, Zebarjad SM et al (2011) Fabrication, characterization, and measurement of viscosity of α-Fe_2O_3-glycerol nanofluids. J Mol Liq 163:27–32
48. Shi B, Sinha S, Dhir VK (2006) Molecular dynamics simulation of the density and surface tension of water by particle-particle particle-mesh method. J Chem Phys 124:204715
49. Mountain RD (2009) An internally consistent method for the molecular dynamics simulation of the surface tension: application to some tip4p-type models of water. J Phys Chem B 113:482–486

50. Zhu RZ, Yang H (2011) A new method for the determination of surface tension from molecular dynamics simulations applied to liquid droplets. Chinese Phys B 20:016801
51. Rutkevych PP, Ramanarayan H, Wu DT (2010) Optimizing the computational efficiency of surface tension estimates in molecular dynamics simulations. Comp Mater Sci 49:s95–s98
52. Hou HY, Chen GL, Chen G (2009) A molecular dynamics simulation on surface tension of liquid Ni and Cu. Comp MaterSci 46:516–519
53. Sunda AP, Venkatnathan A (2013) Parametric dependence on shear viscosity of SPC/E water from equilibrium and non-equilbrium molecular dynamics simulations. Mol Simul 39:728–733
54. Medina JS, Prosmiti R, Villarreal P (2011) Molecular dynamics simulations of rigid and flexible water models: temperature dependence of viscosities. Chem Phys 388:9–18
55. Thomas JC, Rowley RL (2011) Transient molecular dynamics simulations of liquid viscosity for nonpolar and polar fluids. J Chem Phys 134:024526
56. Li X, Hede T, Tu Y (2011) Glycine in aerosol water droplets: a critical assessment of Köhler theory by predicting surface tension from molecular dynamics simulations. Atmos Chem Phys 11:519–527
57. D'Auria R, Tobias DJ (2009) On the relation between surface tension and ion adsorption at the air-water interface: a molecular dynamics simulation study. J Phys Chem A 113:7286–7293
58. Ge S, Zhang XX, Chen M (2011) Viscosity of NaCl aqueous solution under supercritical conditions: a molecular dynamics simulation. J Chem Eng Data 56:1299–1304
59. Chen T, Chidambaram M, Liu ZP et al (2010) Viscosities of the mixtures of 1-ethyl-3-methylimidazolium chloride with water, acetonitrile and glucose: a molecular dynamics simulation and experimental study. J Phys Chem B 114:5790–5794
60. Kumar P, Varanasi SR, Yashonath S (2013) Relation between the diffusivity, viscosity, and ionic radius of LiCl in water, methanol, and ethylene glycol: a molecular dynamics simulation. J Phys Chem B 117:8196–8208
61. Hasan B, Keblinski P, Khodadadi JM (2013) A proof for insignificant effect of Brownian motion-induced micro-convection on thermal conductivity of nanofluids by utilizing molecular dynamics simulations. J Appl Phys 113:084302
62. Mohebbi A (2012) Prediction of specific heat and thermal conductivity of nanofluids by a combined equilibrium and non-equilibrium molecular dynamics simulation. J Mol Liq 175:51–58
63. Cui WZ, Bai ML, Lv JZ (2011) On the influencing factors and strengthening mechanism for thermal conductivity of nanofluids by molecular dynamics simulation. Ind Eng Chem Res 50:13568
64. Li L, Zhang YW, Ma HB et al (2010) Molecular dynamics simulation of effect of liquid layering around the nanoparticle on the enhanced thermal conductivity of nanofluids. J Nanopart Res 12:811–821
65. Teng KL, Hsiao PY, Hung SW et al (2008) Enhanced thermal conductivity of nanofluids diagnosis by molecular dynamics simulations. J Nanosci Nanotech 8:3710–3718
66. Li L, Zhang YW, Ma HB et al (2008) An investigation of molecular layering at the liquid-solid interface in nanofluids by molecular dynamics simulation. Phys Lett A 372:4541–4544
67. Sarkara S, Selvam SP (2007) Molecular dynamics simulation of effective thermal conductivity and study of enhanced thermal transport mechanism in nanofluids. J Appl Phys 102:074302
68. Horn HW, Swope WC, Pitera JW et al (2004) Development of an improved four-site water model for biomolecular simulations: TIP4P-Ew. J Chem Phys 120:9665–9677
69. Ryckaert JP, Ciccotti G, Berendsen HJC (1977) Numerical integration of the cartesian equations of motion of a system with constraints: molecular dynamics of n-alkanes. J Comput Phys 23:327
70. Daw MS, Foiles SM, Baskes MI (1993) The embedded atom method: a review of theory and applications. Mater Sci Rep 9:251–310
71. Schravendijk P, van der Vegt N, Site LD et al (2005) Dual-scale modeling of benzene adsorption onto Ni(111) and Au(111) surfaces in explicit water. Chem Phys Chem 6:1866–1871

72. Plimpton S (1995) Fast parallel algorithms for short-range molecular dynamics. J Comput Phys 117:1–19
73. Ismail AE, Grest GS, Stevens MJ (2006) Capillary waves at the liquid-vapor interface and surface tension of water models. J Chem Phys 125:014702
74. Muller-Plathe F, Bordat P (2002) International summer school on novel methods in soft matter simulations. Helsinki Finland
75. Gittens GJ (1969) Variation of surface tension of water with temperature. J Colloid Interface Sci 30:406–412
76. Hilsenrath J, Klein M, Woolley HW (1955) Tables of thermal properties of gases. National Bureau of Standards Circular, Washington D.C
77. Einstein A (1905) Über die von der molecular kinetischen Theorie der Wärmege forderte Bewegung von in ruhenden Flüssig keiten suspendierten Teilchen. Ann Phys 322:549–560
78. Carré A, Woehl P (2006) Spreading of silicone oils on glass in two geometries. Langmuir 22:134–139